2021 IEEE 18th International Conference on Mobile Ad Hoc and Smart Systems (MASS) | 978-1-6654-4935-9/21/$31.00 ©2021 IEEE | DOI: 10.1109/MASS52906.2021.00059

Crashing Waves: An Empirical Vehicle-to-Barrier Communication Channel Model via Crash Tests

Mohammad M. R. Lunar* Cody Stolle† Ronald K. Faller† Mehmet C. Vuran*
*Cyber-physical Networking Laboratory, Computer Science and Engineering; †Midwest Roadside Safety Facility,
University of Nebraska-Lincoln, Lincoln, NE, USA, Email: mlunar@cse.unl.edu, {cstolle2, rfaller1, mcv}@unl.edu

***Abstract*—Vehicle-to-barrier (V2B) communications is an emerging communication technology between vehicles and roadside barriers to mitigate run-off-road crashes, which result in more than half of the traffic-related fatalities in the United States. To ensure V2B connectivity, establishing a reliable V2B channel is necessary before a potential crash, such that real-time information from barriers can help (semi-)autonomous vehicles make informed decisions. However, the characteristics of the V2B channel are not yet well understood. Therefore, in this paper, a V2B channel model is developed with three channel metrics: received power, root mean square (RMS) delay spread, and RMS Doppler spread based on experiments during controlled vehicle crash tests. Experimentation, empirical analyses, and mathematical models are introduced to capture the impacts of antenna height, barrier type, and vehicle type in V2B channel characteristics. Vehicle-height barrier antennas experience 6.4% (540ns) less reference delay spread while encountering 10% (13Hz) higher reference Doppler spread and 10dB more received power than the barrier-height barrier antennas. Moreover, steel barrier deployment results in a 21% ($2,040$ns) larger reference delay spread and 2.4% (2.35Hz) smaller reference Doppler spread than concrete barrier deployment. Finally, the impact of the crash in the communication channel is investigated with these empirical metrics. To the best of our knowledge, this is the first V2B communication channel model that captures received power, RMS delay spread, and RMS Doppler spread validated with the most extensive set of vehicular crash tests. The experimental code and experiment dataset are made public to support reproducible research (https://github.com/UNL-CPN-Lab/Crashing-Waves).**

I. Introduction

Annually, around 1.35 million people die in road accidents in the World [1], with at least 20 million more people injuring in crashes. According to the world health organization, road crashes become the principal cause of death for people ages 5 to 29 [1]. In the U.S., the number of fatalities due to road crashes has been consistently greater than $32,000$ per year in this decade (e.g., $36,560$ in 2018 [2] and $36,096$ in 2019 [3]). According to the National Highway Traffic Safety Administration statistics, in 2019, 52.59% of fatalities was caused by a single-vehicle crash [4]. In the last decade, this rate has always exceeded 50%. A National Center for Statistics and Analysis study shows that 70% of single-vehicle crashes is caused by run-off-road (RoR) crashes [5].

To eliminate the fatalities in road transport, intelligent transport systems (ITS) are introduced between vehicles and roadside infrastructure. Vehicle-to-everything (V2X) is considered the key to those intelligent systems [6]. Several connected vehicular technologies include: vehicle-to-vehicle (V2V) [7], vehicle-to-infrastructure (V2I) [8], vehicle-to-pedestrian (V2P) [9], vehicle-to-cloud (V2C) [10], and

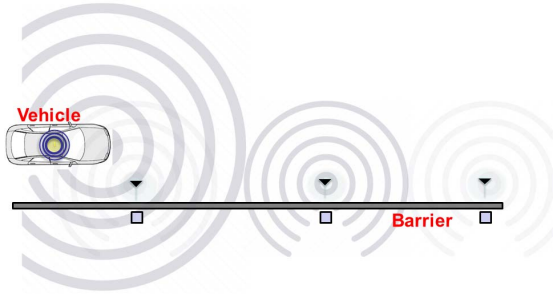

Fig. 1: V2B Communications.

vehicle-to-barrier (V2B) [11]–[13] are introduced in the literature to serve different vehicle consumers' purposes. Mainly V2V and V2I are considered for improving roadside safety and reducing fatalities and injuries on roads.

Intelligent vehicular communication-based roadside safety systems are introduced in the literature and implemented in practice. For example, Toyota has implemented V2V and V2I for its cars in Japan, [14], to reduce the possibility of crashes close to intersections. Similarly, California Partners for Advanced Transit and Highways (PATH) is implementing automatic platooning for trucks by V2V communication [15], to maintain a small constant clearance between trucks on highways without any collisions [16]. However, these solutions mainly focus on multi-vehicular crashes on roads and do not consider the single-vehicle RoR crashes, which result in more than half of the traffic fatalities. To reduce the losses caused by single-vehicle crashes, we introduced a new vehicular communication paradigm, vehicle-to-barrier (V2B) communications [17], for moving vehicles to establish a communication link with roadside barriers (Fig. 1). This link aims to exchange information (e.g., road condition, barrier type, curvature, road type, etc) between the moving vehicle and the barrier to assist the onboard computer or the driver so that a RoR crash can be avoided. A successful deployment of this scheme could potentially replace physical roadside barriers, which are hazards for vehicles, with virtual barriers. We summarize detailed motivation and use-cases of the V2B scheme in [13] and the V2B communication behavior during crash tests is observed in [12], [13].

The aim is to keep vehicles on the road by ensuring interruption-free V2B communication. This interruption-free link can also confirm early detection of a potential RoR crash based on the instantaneous messages received from the vehicles on the road. A major challenge is designing a uniform system that could work regardless of vehicle type, barrier type,

978-1-6654-4935-9/21/$31.00 ©2021 IEEE
DOI 10.1109/MASS52906.2021.00059

roadside shape, and antenna deployment position. In addition, an in-depth investigation for proper barrier design and an emergency message forwarding scheme would also be required in the next phase.

More specifically, for the successful utilization of V2B communications, a detailed analysis of the V2B channel parameters is necessary. In this paper, we aim to bridge this gap. An empirical channel model is presented. Accordingly, RMS delay spread and RMS Doppler spread are also estimated. For all the experiments, the V2B channel behaviors are captured for the vehicle antenna height, vehicle encroachment angle, the distance between the vehicle and barrier antennas, the velocity of the vehicle, and the types of vehicles and barriers. We briefly summarize the contributions as follows:

- Five vehicle crash experiments are conducted with software-defined-radio (SDR) equipment, and the channel metrics: received power, RMS delay spread, and RMS Doppler spread are empirically measured. This is the most comprehensive data set for high-velocity wireless V2B communications to the best of our knowledge.
- We capture these channel metrics through empirical models that are validated based on the experiment results. To the best of our knowledge, this is the first empirical V2B channel model. Dataset[1] and implementation codes[2] for this model are open for everyone in the online public repository.
- Finally, we present the impacts of vehicles and barrier-related parameters on the V2B channel characteristics, which have important implications for the design of V2B systems in practice.

The remainder of the paper is organized as follows: In Section II, the related work is discussed. In Section III, the experiment methodology is explained for both the static open-space tests and the crash tests. Then, the performance metrics measurement and mathematical modeling methodologies are described in Section IV. The evaluation of the V2B channel model with the real-world crash tests is presented in Section V. We conclude the paper in Section VI.

II. Related Work

Physical layer channel metrics analysis is a prevalent approach in literature for investigating wireless channel characteristics. Path loss and delay spread are analyzed for static transmitter and receiver nodes in an expansive range of cases [18]–[20]. In addition, Doppler spread is also investigated for mobile cases [21], [22]. Empirical estimation of these channel metrics is also explored in the literature [23]–[26].

Studies of path loss, delay spread, and Doppler spread have recently gained attention for vehicular communications [27], [28]. These studies assist in developing reliable and efficient vehicular communication solutions. For example, a collection of urban channel measurements for V2I is demonstrated in [29], categorizing the experiment sites into three different regions and modeling the channel metrics for each region. These models are then utilized to evaluate the communication behavior for each region. In [30], channel metrics of a V2I network are presented in a rural environment, classifying the measurements into line-of-sight (LOS) and non-line-of-sight (NLOS) cases. In [31], similar types of measurements are evaluated for the V2V scenario of highway vehicles . However, no communication measurement is available in the literature that addresses single-vehicle, RoR crash conditions.

We observe a similar scenario for commercial standards of vehicular communication solutions. In the sub-6GHz vehicular communication domain, currently dedicated short-range communication (DSRC) [32] and Cellular-V2X (C-V2X) [33] are the two most prominent standards. These communication schemes are used in a wide variety of vehicular applications [34], [35]. However, none of these schemes are investigated in vehicular crash situations.

Previous work on V2B communications describes the effects of various performance metrics such as received signal strength (RSS), error vector magnitude (EVM), signal-to-noise ratio (SNR), and bit error rate (BER) during the crash tests [13]. However, an in-depth analysis of key channel parameters, including path loss, delay spread, Doppler spread, is necessary for efficient and reliable deployment of this mechanism. Furthermore, extensive V2B channel models are missing in the literature. In this paper, we aim to bridge this gap. To the best of our knowledge, this is the first paper that discusses received power, RMS delay spread, and RMS Doppler spread models for the V2B communication channel with the most extensive set of vehicular crash tests.

III. Experiment Methodology

In this section, we discuss the detailed experiment methodology for the wireless experiments, crash tests, and open space experiments conducted at the Midwest Roadside Safety Facility (MwRSF).

A. Wireless Experiment Methodology

We use Ettus Universal Software Radio Peripherals (USRPs) [36]. These radios are placed in vehicles and on or near barriers. The radio devices for the tests are USRP E312, USRP B200, and USRP B210. Their placements in the experiments are discussed in Section III-B. For operating these USRPs, we use GNU Radio $3.7.13.4$ and UHD $3.13.1.0$ [37], [38], and we use GNU Radio's benchmark orthogonal frequency division multiplexing (OFDM) python script [39] with necessary modifications for transmitting and receiving the signals. We set the USRP for transmitting OFDM symbols at 5.8 GHz with a baseband sampling rate of 500 ksps and FFT length of $N_{FFT} = 64$. Of these 64 sub-carriers, 46 are used for communicationm and the remaining are reserved as guard bands and for DC. The cyclic prefix (CP) length is $N_{CP} = 128$, and the signal is modulated with BPSK modulation. The preamble of this OFDM system is block type. Twenty-four consecutive data symbols follow one block-type preamble. We refer to this set of 25 symbols (1 preamble

[1]https://ieee-dataport.org/open-access/crashing-waves-empirical-vehicle-barrier-communication-channel-model-crash-tests

[2]https://github.com/UNL-CPN-Lab/Crashing-Waves

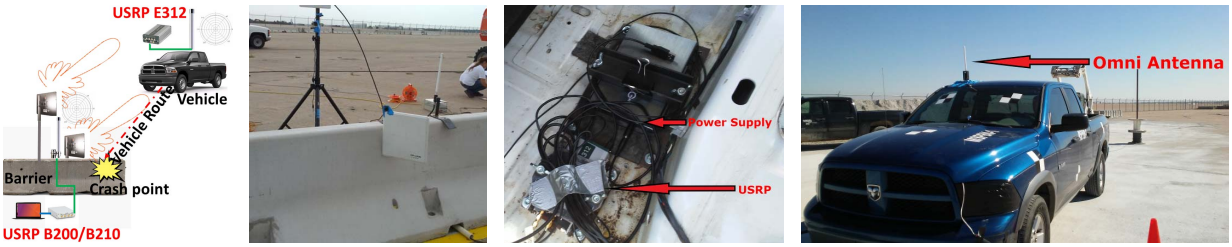

(a) Crash Tests Setup (b) Barrier antennas (c) E312 inside vehicle (d) Vehicle antenna

Fig. 2: Crash Test: Overall setup, barrier antennas, USRP setup inside the vehicle, and vehicle antenna.

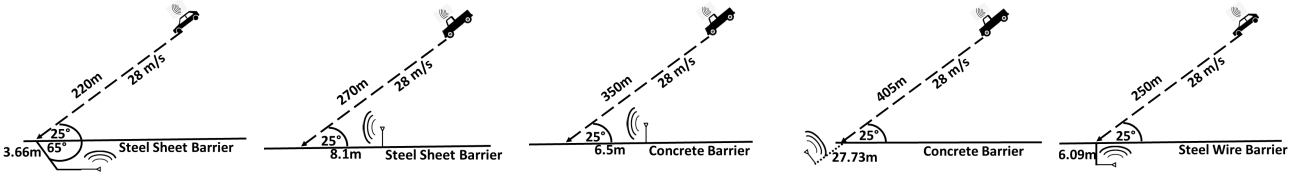

(a) SSSB (b) PSSB (c) PCB (d) PCBL (e) SSWB

Fig. 3: Crash test illustrations: Initial vehicle distance to the barrier impact point, encroachment angle and speed, barrier type, and barrier antenna distance to the impact point are indicated.

TABLE I: Crash Tests Parameters

Test Name	Antenna Height		Antenna Type		Vehicle Type	Barrier Type	Max. Distance	Max. Velocity
	Vehicle	*Barrier*	*Vehicle*	*Barrier*				
SSSB	1.45m	1.45m	Omni	Panel	Sedan	Steel Sheet	220m	28 m/s
		0.87m		Panel				
PSSB	1.8m	1.8m	Omni	Panel	Pickup	Steel Sheet	270m	28 m/s
		0.82m		Omni				
PCB	1.8m	1.8m	Omni	Panel	Pickup	Concrete	350m	28 m/s
		0.82m		Omni				
PCBL	1.88m	1.88m	Omni	Panel	Pickup	Concrete	430m	28 m/s
SSWB	1.45m	1.0m	Omni	Panel	Sedan	Steel Wire	250m	28 m/s

and 24 data symbols) as an OFDM frame in this paper. The receiver uses this block-type preamble for synchronizing the received signal by using the Schmidl and Cox OFDM synchronization algorithm [40]. We select the parameters such that we can observe the channel impact over a simple OFDM signal. ISM 5.8 GHz band is chosen so that the solution could be easily deployed in DSRC equipped vehicles without installing any additional hardware.

B. Crash Test Methodology

Next, we discuss the five real-world crash tests and their technical setup (Fig. 2a), conducted at MwRSF. In each experiment, the barrier antenna's locations are determined based on safety precautions indicated by the expert team from the facility. On the barrier side, we use USRP B200/B210s, which are connected to either a highly directional panel antenna [41] (28 dBi maximum gain) or a dual-band omnidirectional antenna [42] (5.3dBi gain) (Fig. 2b). We refer to the antennas attached to or next to the barrier as the *barrier antenna* throughout the paper. The positions of the antennas are selected for each crash test to minimize the chances that the crash vehicle hits any components. The barrier radio is connected to a laptop operating the B200/B210.

On the vehicle side, we mount a USRP E312 inside a vehicle (Fig. 2c). E312 is a battery-operated portable stand-alone SDR, allowing us to easily set it inside the crash vehicle without any additional computing machines during the operation. The USRP with a backup power bank is placed inside a metal frame and firmly attached to the vehicle body to minimize damage during the crash. None of the devices were damaged during the crash tests.

On the vehicle's rooftop, we place a dual-band omnidirectional antenna (Fig. 2d). This antenna is similar to the omnidirectional barrier antennas. This antenna transmits the OFDM signal from the USRP E312 at a 5.8 GHz frequency. Throughout the paper, we refer to the antenna attached to the vehicle as the *vehicle antenna*. The transmit power of USRP E312 is set to 10dBm for all the experiments. In the experiments, the vehicle antenna is used as the transmitter, and each barrier antenna is used as a receiver. On the barrier, we place antennas at different heights.

Results from a total of five crash tests are presented in this paper. These crash tests are labeled based on the vehicle and barrier types involved: Sedan to Steel Sheet Barrier (SSSB), Pickup to Steel Sheet Barrier (PSSB), Pickup to Concrete Barrier (PCB), Pickup to Concrete Barrier LOS (PCBL), and Sedan to Steel Wire Barrier (SSWB) crash tests.

Table I includes details of each crash test. Geometric details about each test are illustrated in Fig. 3. From the starting point, the crash vehicle is pulled by another vehicle with a pulley. At the end of the trajectory, the cable and pulley of the crash vehicle are released. As a result, the crash vehicle travels the last part of its distance freely and finally crashes to the barrier. The pulling vehicle ensures that the crash vehicle can achieve its desired velocity v. For the experiments we present here,

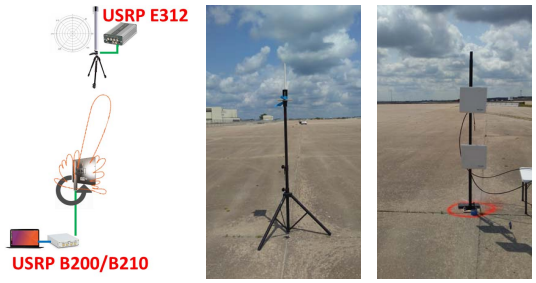

(a) Experiment layout (b) Vehicle-Equiv. (c) Barrier-Equiv.

Fig. 4: Open space experiment setup.

the value of v is 62mph (or 28m/s). The angle between the encroachment trajectory and the barrier is set to 25° for the tests.

Besides the radios and antennas, we use two high-precision accelerometers and three high-resolution cameras to synchronize collected radio data with vehicle position and speed. The accelerometer collects acceleration data at the rate of 10kHz on each axis. The three high-resolution cameras were installed on the spot of the crash test. They are connected with another laptop during the test. The laptops operate the USRP B200/B210, and the cameras are synchronized with the Network Time Protocol (NTP) [43] protocol before each crash test.

C. Static Open-Space Experiment Methodology

The objective of the open-space experiments is to quantify the impact of antenna directivity in overall communication. Therefore for these tests, we consider only directional panel antennas as the barrier antenna. For these tests, we place radios and antennas in the same facility where we conduct crash experiments. Therefore, the large-scale scattering environment is the same as that in crash tests. We place the equipment in an open space where no barrier is positioned. Although there are no barriers in this set of tests, we call these directional antennas barrier-equivalent antennas. Correspondingly, a second setup is called a vehicle-equivalent antenna. To quantify the impact of the vehicle body on the antenna directivity, we conduct two sets of experiments, with and without a vehicle.

In the static experiments (Figs. 4a), we place two barrier-equivalent antennas on one end. Similar to the crash tests, we place them in two different heights: 0.8m as the barrier height and 1.5m as the vehicle height. The vehicle-equivalent antenna is placed at 1.5m. It is placed on a tripod for the no-vehicle experiments and on the rooftop of a sedan for the experiments with the vehicle. The distance between the vehicle-equivalent antenna and the barrier-equivalent antenna varies in an arithmetic progression of 10 values having first term and common difference as 30.48m, i.e., 100ft. At each location, the barrier-equivalent antenna receives signals for 20 secs. For each location, the barrier-equivalent antenna receives signals for 8 different directivity angles. The directivity angle is calculated as the angle between the barrier-equivalent antenna boresight and the line between the vehicle and barrier-equivalent antenna. For this experiment, we select 8 different directivity angles: $0^\circ, 3^\circ, 6^\circ, 10^\circ, 20^\circ, 30^\circ, 60^\circ$, and 90°, where 0° refers to the case when the antenna boresight points to the vehicle. We collect data for both types of tests, i.e., with and without vehicle tests. Therefore for 10 different distances, 8 different angles, and 2 different types, we have a total of 160 cases.

The vehicle-equivalent and barrier-equivalent antennas are shown in Figs. 4b and 4c. In Fig. 4c the barrier-equivalent antenna is placed in a base that can rotate. For the case of vehicle experiments, the vehicle-equivalent antenna setup is the same as the vehicle antenna setup of the crash test in Fig. 2d. Next, we discuss the methodology for processing the collected experimental data.

IV. Measurement Methodology and Modeling

In the following, we discuss the methodology to obtain relevant channel and experiment parameters and the channel model. More specifically, OFDM demodulation and channel frequency response (CFR), received power modeling, RMS delay spread, RMS Doppler spread, and experiment parameter calculation procedures are described.

A. OFDM Demodulation and CFR

The transmitted OFDM signal from the vehicle is received by the barrier radios and synchronized with Schmidl and Cox OFDM synchronization algorithm [40]. The synchronized and CP-separated received IQ stream is converted to frequency domain data through FFT operation by the benchmark OFDM receiver code and stored as log files. As a result, CFR can be calculated from frequency domain log files.

The transmitted signal contains a sequence of OFDM frames, consisting of one block type preamble and 24 data symbols. For each preamble, we use the least square (LS) channel estimation [44] to estimate the channel. This preamble works as a block-type pilot. This block-type pilot is then used to estimate the channel of the next symbol. This estimate is then used to estimate the following symbol. In this way, the header of the OFDM frame is estimated and then demodulated. This methodology is performed to track the rapid channel variations more accurately instead of conventionally relying on the pilot sequence for the entire frame. Since all the transmitted data is known at the receiver, channel estimation can be performed at a symbol granularity.

The header of the demodulated OFDM symbol contains the frame index. This frame index is used to identify the missing frames. The channel of the missing frame is then indicated as a null stream in the overall estimated channel.

B. V2B Channel Model

In this section, the V2B channel model is presented. A modified log-distance received power model is considered for the V2B channel. The classical equation for modeling log distance received power and widely used in the literature [45], [46] has several limitations. This model assumes that the received power is independent of the antenna, antenna gain, and the angle between the transmitter and receiver. However, this assumption does not hold in practice, especially with directional antennas, which strongly impact the propagation of signals.

For the V2B channel, we define the received power as follows:

$$\begin{aligned} P_r(d,\theta,h_V,h_B) = P_{r_0}(h_V,h_B) - 10\eta(h_V,h_B)\log\left(\frac{d}{d_0}\right) \\ + w_k K(d,\theta,h_V,h_B) \\ + w_v V(d,\theta,h_V,h_B) \\ + w_{h_B}\log h_B + w_{h_V}\log h_V + w_b \\ - L_d(d,h_V,h_B) - \Gamma(d,h_V,h_B,\theta), \end{aligned} \tag{1}$$

where the first two terms are the classical log distance received power model, $P_{r_0}(h_V,h_B)$ is the reference received power of the model at distance d_0; θ is the angle between vehicle and barrier; received power exponent is $\eta(h_V,h_B)$, $K(d,\theta,h_V,h_B)$ and $V(d,\theta,h_V,h_B)$, and w_k and w_v are the correction factors and associated weights for antenna directionality and the vehicle body, respectively; h_V and h_B are vehicle and barrier antenna heights; w_{h_V} and w_{h_B} are their weights; w_b is the bias; $L_d(d,h_V,h_B)$ and $\Gamma(d,h_V,h_B,\theta)$ are the diffraction and reflection losses due to the barrier, respectively. The reference distance, d_0, is set to $30.48m$.

We discuss each term in (1) in the following. Empirical data collected in Section III-C are utilized for this model development.

Log Distance Received Power: Received signal powers are evaluated for specific d, θ, h_V, and h_B according to the empirical data. Received power exponent $\eta(h_V,h_B)$ is calculated from the empirical received power data without a vehicle at LOS condition, i.e., $\theta = 0°$. For each h_V and h_B, the corresponding $\eta(h_V,h_B)$ is determined for the model.

Model for K & V: We include $K(d,\theta,h_V,h_B)$ in (1). This quantity was introduced [23] for addressing antenna directivity in the path loss model. For the V2B scheme, the vehicle antenna is considered Omnidirectional. Therefore K is defined to only address the barrier antenna directivity. If the barrier antenna is Omni-directional, as in some of our experiments, we set $\theta = 0°$.

For the V2B received power model, addressing antenna directivity is not sufficient. From the static open-space experiments, we observe that the vehicle body significantly influences path loss. Therefore, we have also modified Kelner's approach with an additional correction factor, $V(d,\theta,h_V,h_B)$.

The correction factors $K(d,\theta,h_V,h_B))$ and $V(d,\theta,h_V,h_B))$ are empirically determined from the static open-space experiments as follows: Using experiments without the vehicle (i.e., $V(d,\theta,h_V,h_B) = 0$), the measured received power, $P_r(d,\theta,h_V,h_B)$ is used to find $K(d,\theta,h_V,h_B) = P_r(d,\theta,h_V,h_B) - P_r(d,0,h_V,h_B)$ according to [23]. Therefore, the difference between the received power of the current directivity angle and the received power when the directivity angle is $0°$ denotes the correction factor. Similarly, $V(d,\theta,h_V,h_B)$ is calculated by comparing experiments with and without the vehicle for d, h_V, h_B, and θ. Then, these values are interpolated for any d and θ.

From the empirical data, K and V values are available for a specific combination of d and θ. To evaluate K and V for any d and θ we model these two quantities as a function of d, h_V, h_B and θ by utilizing the empirical data. Accordingly, the mathematical model of K and V are:

$$\begin{aligned} K(d,\theta,h_V,h_B) = w_{kd}\log(d) + w_{kh_B}\log(h_B) \\ + w_{kh_V}\log(h_V) + w_{k\theta}\theta + w_{kb}\ , \end{aligned} \tag{2}$$

$$\begin{aligned} V(d,\theta,h_V,h_B) = w_{vd}\log(d) + w_{vh_B}\log(h_B) \\ + w_{vh_V}\log(h_V) + w_{v\theta}\theta + w_{vb}\ , \end{aligned} \tag{3}$$

where w_{kd}, w_{kh_V}, w_{kh_B} $w_{k\theta}$, w_{vd}, w_{vh_B}, w_{vh_V} and $w_{v\theta}$ are the weights and w_{kb} and w_{vb} are the biases. Here the unit of θ is radian and the units of d, h_V, and h_B are meter.

These weights and biases are calculated using least square multiple regression. Using the empirical data, we found the values as: $w_{kd} = 2.38$, $w_{kh_V} = -12.44$, $w_{k\theta} = -11.32$, $w_{kb} = -6.47$, $w_{vd} = -3.26$, $w_{vh_V} = 2.35$, $w_{v\theta} = -1.59$, and $w_{vb} = 21.76$. For evaluating empirical data, we use only one vehicle (i.e., only one value of h_V). Therefore, w_{kh_V}, and w_{vh_V} are zero for this case and the contribution of vehicle height is summed as a constant value with the biases.

Diffraction Loss (L_d) and Reflection Loss (Γ): During the crash tests, the barrier can contribute as the source of diffraction and reflection losses. We model these losses with received power in (1). Diffraction loss L_d is modeled with classical knife-edge diffraction model [47] assuming barrier top corner as a knife-edge. On the other hand, reflection loss is modeled from reflection coefficient [48], based on the barrier top surface's reflection and refraction properties. Since static open-space tests are conducted without barriers, these losses are zero for those experiments.

Model Weights (w_k, w_v) & Bias (w_b): Using all the components in (1), the estimated received power can now be evaluated for known d, h_V, h_B, θ values from the model. From empirical values of static open-space tests these weights and biases can be derived using least square multiple regression algorithm. The calculated values are: $w_k = 1.64$, $w_v = -0.55$, $w_{h_B} = 3.15$ and $w_b = 11.08$.

RMS error of this fit is: 4.09dB and R^2 value is 0.63. On the other hand, RMS error of fit (2) and (3) are: 6.01dB and 6.59dB and R^2 values are 0.49 and 0.03 respectively. To avoid over-fitting, we accept small R^2 values in (2) and (3) compared to a traditional regression model. This results a better overall fit for (1).

Log Normal Random Fading Model: So far, fading has not been considered. Accordingly, (1) can be modified to capture log-normal fading as:

$$X_\sigma = P_{r_E}(d,\theta,h_V,h_B) - P_r(d,\theta,h_V,h_B)\ , \tag{4}$$

where σ is the standard deviation of fading, P_{r_E} is the empirical received power, and $P_r(d,\theta,h_V,h_B)$ is given in (1).

We also represent a hypothesis testing about the observation that the measured fading of the model is not lognormal and then calculate the p-values of this hypothesis for each experiment.

C. RMS Delay Spread

We use the frequency domain channel state information (CSI), i.e., CFR, for calculating the RMS delay spread. First, we calculate the power delay profile (PDP), from which we empirically quantify the RMS delay spread.

Before utilizing CFR for PDP, the phase errors within CFR need to be corrected. Therefore we apply the phase correction approaches on CFR based on the methodologies in the literature [24], [25]. These approaches are discussed below.

Non-linearity of the radio components: Different components of the radio device creates non-linear errors in the signal, which exhibit non-linear phase errors in CFR. To remove this non-linearity, we use least-square linear regression [24] for the 46 occupied sub-carriers of the OFDM signal, which is implemented for each OFDM symbol.

Uncertainty of the frame synchronization starting point: To avoid the inter-symbol interference (ISI), OFDM signals use CP. The OFDM synchronizes the block type preamble and then demodulates the signal. Since the preamble is also cyclic-prefixed with N_{CP} sub-carriers, there is an uncertainty of time $t_u = t_s \times N_{CP}$, where t_s is the sampling time of a sample. This timing uncertainty in the time domain produces a phase offset in the frequency domain. According to [49], this phase offset follows a Gaussian distribution (with zero mean). We split the vehicle's overall encroachment path into several different slices with 50m intervals for the crash tests. At each 50m interval, we take the average of the phase of CFR frames to reduce the phase offset close to zero.

Carrier frequency offset (CFO): CFO occurs in a wireless system, mainly for two reasons: (1) For the two different USRPs, the carrier frequency cannot be perfectly the same. (2) Doppler effect creates a frequency shift. The Schmidl and Cox OFDM synchronizer [40] also addresses the CFO error and corrects it. Therefore, we do not take any additional steps to correct the CFO.

After the phase corrections, the CFR is converted into the time domain by IFFT. This makes a channel impulse response (CIR) representation of the signal. This CIR is then used to find the PDP, which is used for RMS delay spread.

To calculate the empirical values of RMS delay spread, first, the spurious components are extracted from the PDP with a threshold of 15dB from the maximum value. This threshold is chosen based on the average SNR value of the signals. Then, the RMS delay spread is calculated as [48]:

$$\tau_{RMS} = \sqrt{(\widetilde{\tau^2}) - (\widetilde{\tau})^2} \ , \tag{5}$$

where $\widetilde{\tau} = \sum_k P_k \tau_k / \sum_k P_k$ and $\widetilde{\tau^2} = \sum_k P_k \tau_k^2 / \sum_k P_k$, and P_k is the absolute power of the k-th frame of PDP.

Using the empirical RMS delay spread values of all crash tests, we depict a mathematical model of RMS delay spread. This RMS delay spread is a function of distance d. The lognormal characteristics of RMS delay spread are observed in the literature [50], [51]. Accordingly, we consider the following model:

$$\tau_{RMS} = T_0 d^{\epsilon} y_{\tau} \ , \tag{6}$$

where T_0 is the reference value of the delay spread, d is the distance between the vehicle and barrier antennas, ϵ is the delay spread exponent, and y_{τ} represents the amount of error in the model. We evaluate this model in Section V.

D. RMS Doppler Spread

Next, we present a mathematical model for RMS Doppler spread based on empirical data. For OFDM signals, we first convert the CFR into time-domain CSI using IFFT. We use empirical and theoretical definitions of the channel auto-correlation function (ACF) to find the Doppler shift [52], [53]. More specifically, empirical ACF is given as [52]:

$$\widetilde{ACF}(m,n) = E(h[m] * conj(h[n])) \ , \tag{7}$$

where $h[m]$ and $h[n]$ are time-domain CSI of m-th and n-th symbol of a frame, respectively. For the 25 symbols in each frame in the system, a total of $25 \times 25 = 625$ different ACF values can be obtained for each frame. The theoretical ACF is given as [52]:

$$ACF(i, i+s) = J_0(2\pi f_d s T_s) \ , \tag{8}$$

where $J_0(\cdot)$ is the zeroth-order Bessel function of the first kind, f_d is the Doppler shift frequency, T_s is the sample time for each symbol, and s is the symbol difference, i.e., the difference between the two symbols whose auto-correlation is calculated.

We calculate the empirical ACF matrix for each OFDM frame for the crash experiments and follow a numerical approach to calculate f_d from ACF based on (8). Accordingly, we find out the maximum range of Doppler frequency from the following equation:

$$f_{d_{max}} = \frac{v_{max} \times f}{c} \ , \tag{9}$$

where v_{max} is the maximum possible velocity of the vehicle, f is the center frequency, and c is the speed of the light. For the crash experiments, $v_{max} = 28$m/s, and $f = 5.8$GHz. From (9), we find $f_{d_{max}}$ as 541.33 Hz. We select roughly $10,000$ linear spaced points within this maximum Doppler range. The range of symbol difference could be $0 \leq s \leq 24$. Therefore for each 25 symbol differences, we take the Bessel function values of all the velocities. As a result, now we have a total of $25 \times 10,000 = 25,000$ values, based on which we calculate the empirical value of f_d. Accordingly, we create an f_d matrix similar to the empirical ACF matrix. Then, the RMS Doppler spread is calculated by taking the RMS of the corresponding vector.

Since the lognormal nature is observed for RMS Doppler spread with velocity in literature, [30], [54], [55] we consider the following model:

$$f_{dRMS} = F_0 v^e y_d \ , \tag{10}$$

F_0 is the reference value of the Doppler spread, v is the vehicle's velocity, e is the Doppler spread exponent, and y_d represents the amount of error in the model. We discuss the effectiveness of this model in Section V.

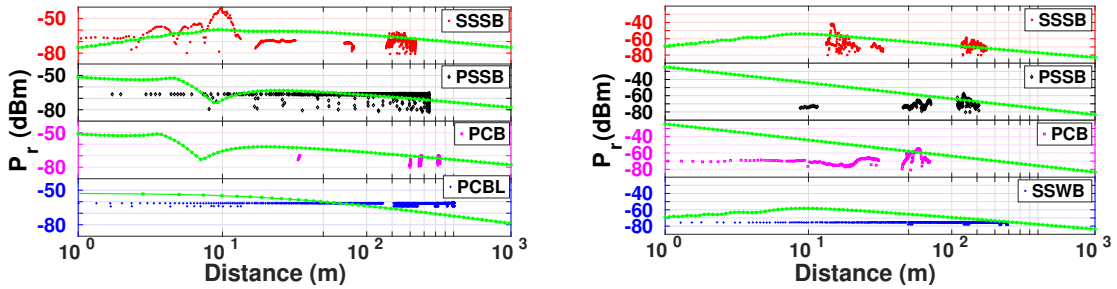

(a) Vehicle-height barrier received power

(b) Barrier-height barrier received power

Fig. 5: Empirical Received Power Values and Corresponding Estimation from Model (Model is marked with green line).

TABLE II: RMS Error of Received Power Model in dB & p-values for Log Normal Random Fading

Test Name	$d > 50$m		$d \leq 50$m		Overall		p-values	
	Vehicle-height	***Barrier-height***	***Vehicle-height***	***Barrier-height***	***Vehicle-height***	***Barrier-height***	***Vehicle-height***	***Barrier-height***
SSSB	5.38	3.83	9.09	11.11	6.44	8.23	0.9998	1
PSSB	4.12	10.06	5.44	24.22	4.37	12.40	0.8673	0.9999
PCB	3.31	8.91	8.39	26.18	3.65	21.94	1	1
PCBL	6.33	-	9.77	-	6.51	-	0.9957	-
SSSW	-	3.66	-	13.41	-	5.11	-	0.9879

E. Velocity, Distance, and Directivity Angle

We employ a methodology for measuring the velocity, distance, and directivity angle of the vehicle precisely. We achieve this precision using the high-precision accelerometer, which is discussed in Section III-B. The filtered accelerometer data is cumulatively integrated with respect to time to calculate the velocity. This velocity is cumulatively integrated to obtain the distance between the vehicle and barrier.

For all the crash tests, the directional panel antenna is placed towards the initial vehicle location. When the vehicle starts moving, the directivity angle also dynamically changes (except PCBL, as mentioned in Section III-B). Since we have the precise position information from the accelerometer data, we can exploit that information to calculate the directivity angle by applying trigonometric analysis. Based on the methodology to analyze the V2B channel metrics as explained in this section, next, we discuss evaluation results.

V. Evaluation Results

In the following, model validation and evaluation results for received power, RMS delay spread, and RMS Doppler spread of the V2B channel are discussed.

A. Received Power

To validate the received power model for V2B communication in (1), all crash experiments are categorized into two parts based on the barrier antenna deployment height. Barrier antennas deployed in height $h > 1m$ are considered vehicle-height barrier antenna deployment, based on the height of the vehicle. On the other hand, barrier antennas deployed in height $h \leq 1m$ are considered barrier-height barrier antenna deployment, based on the barrier height. The specific heights are shown in Table I.

In the vehicle-height (Fig. 5a) and barrier-height (Fig. 5b) barrier antenna results, the distance in the figures (x-axis) is the straight line distance between the vehicle and the barrier. Received power exponents for vehicle-height and barrier-height deployments are 1.68 and 1.96, respectively. For the discussion, we split the overall trajectory into two parts: $d > 50$m and $d \leq 50$m. Vehicle-height deployments have a 10dB higher average received power than barrier-height deployments.

We summarize the difference between empirical received power and modeled values as errors in Table II to analyze these results. p-values of the null hypothesis that this error follows Gaussian distribution with 95% confidence interval is also mentioned in the same table. For $d > 50$m, mean RMS error varies between 3.31dB to 10.06dB. For $d \leq 50$m and directional barrier antenna, this range is 5.44dB to 13.41dB. Omni-directional barrier antennas (barrier-height PSSB and PCB) experience larger RMS mean errors than others due to the lower gain of the omnidirectional antenna. On the other hand, p-values for all experiments ≥ 0.8673 proves the effectiveness of the model.

B. RMS Delay Spread

We classify the entire experiment dataset in these three dimensions to analyze the impacts of barrier antenna height, vehicle type, and barrier type on the RMS delay spread (RDS). Barrier antenna height classification is similar to the classifications of Section V-A. Moreover, we classify the entire crash test delay spread dataset based on vehicle type (sedan and pickup) and barrier type (concrete and steel). The results are shown in Figs. 6.

We summarize the resulting model parameters for RMS delay spread in Table III. We observe a 6.4% smaller reference delay spread for the vehicle-height deployment for vehicle-height and barrier-height barrier antenna experiments (Figs. 6a-6b). In addition, the barrier-height antenna exhibits a negative exponent, meaning the RMS delay spread gradually increases for the barrier-height antenna when the vehicle approaches the barrier. As a result, the barrier-height antenna

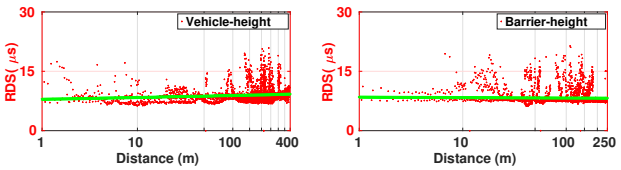

(a) Vehicle-height

(b) Barrier-height

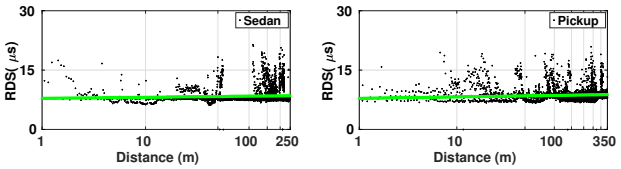

(c) Sedan (d) Pickup

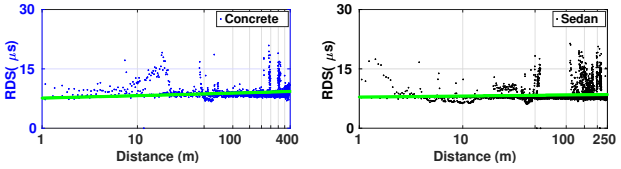

(e) Concrete (f) Steel

Fig. 6: RMS Delay Spread results (Model is marked with a green line).

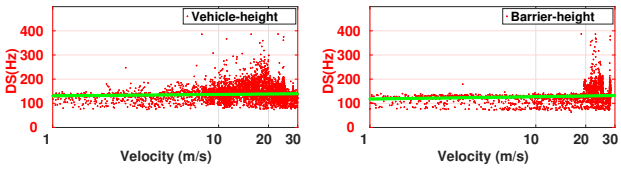

(a) Vehicle-height

(b) Barrier-height

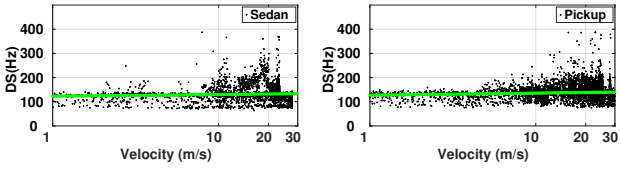

(c) Sedan (d) Pickup

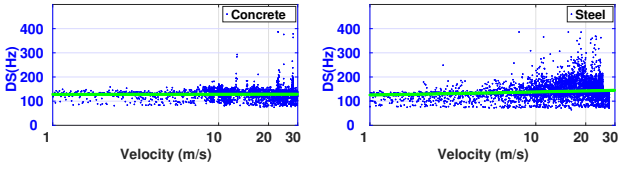

(e) Concrete (f) Steel

Fig. 7: RMS Doppler Spread results (Model is marked with a green line).

TABLE III: RMS Delay Spread Model Parameters

Category	T_0 (μs)	ϵ	σ_{y_τ} **(dB)**
Vehicle-height	7.92	0.03	4.03
Barrier-height	8.46	-0.006	5.42
Sedan	7.87	0.02	5.88
Pickup	7.85	0.02	4.55
Concrete	7.61	0.03	4.38
Steel	9.65	-0.04	7.92

TABLE IV: RMS Doppler Spread Model Parameters

Category	F_0 (Hz)	e	σ_{y_d} **(dB)**	**Kurtosis**
Vehicle-height	130.99	0.019	0.93	4.30
Barrier-height	117.69	0.03	1.0437	4.40
Sedan	123.03	0.02	1.12	3.83
Pickup	127.40	0.03	0.89	4.62
Concrete	128.02	0.002	0.76	5.49
Steel	125.67	0.04	1.08	3.78

experiences greater multi-path effects when the vehicle approaches closer to the barrier.

Similarly, experiments with concrete barriers experience a 21.21% smaller reference delay than those with the steel barrier (Figs. 6e-6f). Moreover, the negative delay spread exponents of steel deployment prove larger multi-path effects near the barrier region. This significant difference suggests potential directions for barrier-specific V2B communication design. For sedan and pickup classification, the difference of reference delay is only 19s (Figs. 6c-6d). Both of them have a decreasing delay effect towards the barrier due to the positive delay spread exponent.

The standard deviation of the mathematical model error, σ_{y_τ} is less than 8dB for all the measurements (Table III) and shows a good agreement with the model [50].

C. RMS Doppler Spread

We discuss the Doppler spread (DS) results, as shown in Figs. 7, using the same classification in Section V-B. The resulting parameters are shown in Table IV. Placing barrier antennas at a vehicle height results in 10% more reference Doppler shift frequency than the barrier-height deployments (Figs. 7a-7b). We also observe a 3.15% increase in reference Doppler shift for pickups compared to sedans (Figs. 7c-7d), resulting in both vehicle and barrier antennas to experience larger Doppler shifts. Moreover, the concrete barrier gets 2.4% more reference Doppler shift than the steel barrier (Figs. 7e, 7f).

Besides, we also include σ_{y_d} and $Kurtosis$, k for Doppler spread in Table IV. It can be observed that the standard deviation of the model error is less than 1.2dB for all cases, which shows an extremely well agreement with the model. The error of this Doppler spread model is reported to be of a Gaussian nature [30], [54]–[57]. Accordingly, the Kurtosis column in Table IVshows that k is within the range of $3.78 \leq k \leq 5.49$, which is inside an acceptable interval [58], while not exhibiting a perfectly Gaussian nature (i.e., $k \neq 3$).

VI. Conclusions

This paper investigates three important channel parameters: path loss, RMS delay spread, and RMS Doppler spread for V2B communication in vehicular crash scenarios. We develop a V2B path loss model as a function of directivity angle (for directional antennas) and vehicular attenuation with distance. Moreover, we derive mathematical models to capture the RMS delay spread and RMS Doppler spread. The comparison between vehicle-height barrier antenna and barrier-height barrier antenna path loss, RMS delay spread, RMS Doppler spread provides key design considerations for practical V2B deployment. The critical regions are also highlighted to motivate further research. RMS delay spread and RMS Doppler spread-based analysis present important

insights about communication performances for vehicle types and barrier types. Finally, a detailed picture is depicted about vehicle-to-barrier communication channels for augmenting the efforts of preventing single-vehicle RoR crashes.

REFERENCES

[1] World Health Organization, "Global status report on road safety 2018," https://apps.who.int/iris/bitstream/handle/10665/277370/WHO-NMH-NVI-18.20-eng.pdf, 2018, accessed: 2020-08-13.

[2] NHTSA, "Traffic deaths decreased in 2018, but still 36,560 people died," https://www.nhtsa.gov/traffic-deaths-2018, 2018, accessed: 2020-07-27.

[3] NHTSA, "Early Estimate of Motor Vehicle Traffic Fatalities in 2019," https://crashstats.nhtsa.dot.gov/Api/Public/ViewPublication/812946.

[4] NHTSA, "Fatality analysis reporting system (FARS)," https://www.nhtsa.gov/research-data/fatality-analysis-reporting-system-fars, 2018, accessed: 2020-08-06.

[5] NHTSA, "Factors related to fatal single-vehicle run-off-road crashes," https://crashstats.nhtsa.dot.gov/Api/Public/ViewPublication/811232, 2020, accessed: 2021-05-27.

[6] K. Abboud et al., "Interworking of DSRC and Cellular Network Technologies for V2X Communications: A Survey," *IEEE Tran. on Vehicular Tech.*, vol. 65, no. 12, pp. 9457–9470, Dec 2016.

[7] A. F. Molisch et al., "A survey on vehicle-to-vehicle propagation channels," *IEEE Wireless Comm.*, vol. 16, no. 6, December 2009.

[8] T. Sukuvaara and P. Nurmi, "Wireless traffic service platform for combined vehicle-to-vehicle and vehicle-to-infrastructure communications," *IEEE Wireless Comm.*, vol. 16, no. 6, pp. 54–61, 2009.

[9] N. Liu et al., "When Transportation Meets Communication: V2P over VANETs," in *Distributed Computing Systems (ICDCS), 2010 IEEE 30th International Conference on*, June 2010, pp. 567–576.

[10] R. Hussain et al., "Rethinking vehicular communications: Merging vanet with cloud computing," in *IEEE 4th International Conference on CloudCom*, Dec 2012, pp. 606–609.

[11] S. Temel, M. Vuran, and R. Faller, "A primer on vehicle-to-barrier communications: Effects of roadside barriers, encroachment, and vehicle braking," *IEEE VTC*, 2017.

[12] S. Temel, M. Vuran, M. Lunar, R. Faller, and C. Stolle, "Vehicle-to-barrier communication during real-world vehicle crash tests," in *IEEE Vehicular Networking Conference, VNC*, 2016.

[13] S. Temel, M. C. Vuran, M. M. Lunar, Z. Zhao, A. Salam, R. K. Faller, and C. Stolle, "Vehicle-to-barrier communication during real-world vehicle crash tests," *Computer Communications*, vol. 127, 2018.

[14] Automotive Industry Portal MarkLines, "Toyota ITS Connect: New system equipped in Prius and other models ," https://www.marklines.com/en/report_all/rep1487_201604, 2016.

[15] Ins. of Transp. Studies, UC Berkeley, "Truck platooning," http://www.path.berkeley.edu/research/automated-and-connected-vehicles/truck-platooning, 2020, accessed: 2021-06-06.

[16] J. Trop, "Volvo Trucks, FedEx Demo Platooning Tech on North Carolina Interstate," https://www.trucks.com/2018/06/28/volvo-trucks-fedex-platooning-tech/, 2018, accessed: 2021-05-06.

[17] S. Temel, M. C. Vuran, and R. K. Faller, "A primer on vehicle-to-barrier communications: Effects of roadside barriers, encroachment, and vehicle braking," in *2016 IEEE 84th Vehicular Technology Conference (VTC-Fall)*, 2016, pp. 1–7.

[18] Zhilong Jiang et al., "Experimental multipath delay spread and path loss analysis for the indoor environment at 5.9 GHz," in *2016 WiSPNET*.

[19] S. Salous and S. El-Faitori, "Path loss models and delay spread parameters for the millimetre wave channel in indoor environments," in *14th EuCAP*, 2020, pp. 1–3.

[20] H. Shimizu et al., "LOS and NLOS path-loss and delay characteristics at 3.35 GHz in a residential environment, year=2000," in *IEEE Antennas and Prop. Society Intl. Symposium.*, vol. 2, pp. 1142–1145 vol.2.

[21] Z. Sharif and A. Z. Sha'ameri, "Estimation of the doppler spread and time delay spread for the wireless communication channel," in *2010 Intl. Conf. on Computer Applications and Industrial Elec.*, 2010.

[22] Gao Yuan et al., "Doppler spread estimation for non-rayleigh fading channel," in *2009 4th IEEE Conf. on Industrial Electronics and Applications*, May 2009, pp. 1106–1109.

[23] J. Kelner and C. Ziółkowski, "Path loss model modification for various gains and directions of antennas," in *12th EuCAP 2018*, April 2018.

[24] Y. Xie et al., "Precise power delay profiling with commodity wi-fi," *IEEE Trans. on Mobile Comp.*, vol. 18, no. 6, June 2019.

[25] Y. Zhuo et al., "Perceiving accurate CSI phases with commodity WiFi devices," in *IEEE INFOCOM*, May 2017, pp. 1–9.

[26] J. Xu et al., "Doppler Effect Mitigation over Mobile Underwater Acoustic OFDM System," ser. WUWNet '18, 2018.

[27] L. Cheng et al., "Comparison of radio frequency and visible light propagation channel for vehicular communications," ser. CarSys, 2016.

[28] D. Jordan et al., "Poster: Investigating doppler effects on vehicle-to-vehicle communication: An experimental study," ser. CarSys '17, 2017.

[29] L. Wang et al., "Vehicle-to-infrastructure channel characterization in urban environment at 28 GHz," *China Communications*, vol. 16, 2019.

[30] W. Li et al., "Path loss models for ieee 802.15.4 vehicle-to-infrastructure communications in rural areas," *IEEE IoT Journal*, vol. 5, no. 5, 2018.

[31] A. Paier et al., "Car-to-car radio channel measurements at 5 GHz: Pathloss, power-delay profile, and delay-Doppler spectrum," in *2007 4th Intl. Symp. on Wireless Comm. Sys.*, 2007, pp. 224–228.

[32] J. B. Kenney, "Dedicated Short-Range Communications (DSRC) Standards in the United States," *Proc. of the IEEE*, vol. 99, no. 7, 2011.

[33] R. Weber et al., "C-V2X - A Communication Technology for Cooperative, Connected and Automated Mobility," in *Mobile Communication - Technologies and Applications; 24. ITG-Symposium*, 2019, pp. 1–6.

[34] 5GAA 2019, "C-V2X Use Cases: Methodology, Examples and Service Level Requirements," https://5gaa.org/wp-content/uploads/2019/07/5GAA_191906_WP_CV2X_UCs_v1-3-1.pdf.

[35] Qualcomm, "Qualcomm 9150 C-V2X chipset," https://www.qualcomm.com/invention/5g/cellular-v2x, 2019.

[36] "Ettus Res." https://www.ettus.com/about, 2020, accessed: 2021-05-08.

[37] Ettus Research, "UHD," https://kb.ettus.com/UHD/, 2020.

[38] GNU Radio, "GNU Radio Website," https://www.gnuradio.org/, 2020.

[39] GNURadio, "OFDM benchmark," https://github.com/gnuradio/gnuradio/tree/maint-3.7/gr-digital/examples/ofdm, accessed: 2021-06-05.

[40] T. Schmidl and D. Cox, "Robust frequency and timing synchronization for OFDM," *IEEE Trans. on Comm.*, vol. 45, no. 12, pp. 1613–1621, 1997.

[41] TPLink, "TL-ANT5823B Datasheet," http://www.linkdataguard.com/datasheets/Wireless/TL-ANT5823B_V1_Datasheet.pdf, 2021-06-07.

[42] Air802 , https://www.air802.com/Dual-Band-Mesh-Omni-Directional-Antenna-2.4-and-5-GHz-Dual-Frequency-N-Female-Connector.html, Omni Antenna Spec. Accessed: 2020-08-08.

[43] NTP, "NTP: The Network Time Protocol," https://www.ntp.org/, 2020.

[44] Y. Shen and E. Martinez, "Channel Estimation in OFDM Systems," Freescale Semiconductor Application Note: AN3059, Jan. 2006.

[45] S. Widodo et al., "Outdoor propagation modeling for wireless sensor networks 2.4 GHz," in *Comnetsat*, 2017, pp. 158–162.

[46] K. Haneda et al., "Frequency-agile pathloss models for urban street canyons," *IEEE Trans. on Antennas and Prop.*, vol. 64, no. 5, 2016.

[47] ITU, "Propagation by diffraction," https://www.itu.int/dms_pubrec/itu-r/rec/p/R-REC-P.526-14-201801-I!!PDF-E.pdf, 2018, accsd: 2021-06-01.

[48] T. Rappaport, *Wireless Communications: Principles and Practice*, 2nd ed. USA: Prentice Hall PTR, 2001.

[49] M. Speth et al., "Optimum receiver design for wireless broad-band systems using OFDM. I," *IEEE Trans. on Comm.*, vol. 47, no. 11, 1999.

[50] K. Tsioumparakis et al., "Delay-spread considerations of same-frequency repeaters in wideband channels," *IEEE Trans. on Vehicular Tech.*, vol. 46, no. 3, 1997.

[51] J. Kim et al., "The distance characteristics of R.M.S. delay spread at urban low-rise environment," in *2016 ICTC*, 2016, pp. 1020–1022.

[52] T. Yucek et al., "Doppler spread estimation for wireless OFDM systems," in *IEEE Symp. on Adv. in Wired and Wireless Comm.*, 2005.

[53] W. Hadiansyah et al., "Doppler spread estimation for OFDM systems using Phase Difference method in Rayleigh fading channels," in *International Conf. on TSSA*, 2012, pp. 147–152.

[54] M. Yusuf et al., "Experimental Characterization of V2I Radio Channel in a Suburban Environment," in *EuCAP*, 2019, pp. 1–5.

[55] Y. Shui et al., "Vehicle-to-Vehicle Radio Channel Characteristics for Congestion Scenario in Dense Urban Region at 5.9 GHz," *Intl. Journal of Antennas and Prop.*, vol. 2018, no. 1751869,, 2018.

[56] L. Bernado et al., "In-tunnel vehicular radio channel characterization," in *IEEE VTC Spring*, 2011, pp. 1–5.

[57] J. Kunisch and J. Pamp, "Wideband Car-to-Car Radio Channel Measurements and Model at 5.9 GHz," in *2008 IEEE VTC*, 2008, pp. 1–5.

[58] T. A. Brown, "Confirmatory factor analysis for applied research," 2006.